Measurements of the energy band gap and valence band structure of $AgSbTe_2$

V. Jovovic
Department of Mechanical Engineering, The Ohio State University, Columbus, Ohio 43210, USA

J. P. Heremans
Department of Mechanical Engineering and Department of Physics, The Ohio State University, Columbus, Ohio 43210, USA

(Received 31 March 2008; published 10 June 2008)

The de Haas-van Alphen effect, galvanomagnetic and thermomagnetic properties of high-quality crystals of $AgSbTe_2$ are measured and analyzed. The transport properties reveal the material studied here to be a very narrow-gap semiconductor ($E_g \approx 7.6 \pm 3$ meV) with $\sim 5 \times 10^{19}$ cm^{-3} holes in a valence band with a high density of states and thermally excited $\sim 10^{17}$ cm^{-3} high-mobility (2200 cm^2/Vs) electrons at 300 K. The quantum oscillations are measured with the magnetic field oriented along the $\langle 111 \rangle$ axis. Taken together with the Fermi energy derived from the transport properties, the oscillations confirm the calculated valence band structure composed of 12 half-pockets located at the *X*-points of the Brillouin zone, six with a density-of-states effective mass $m^*_{da} \geqslant 0.21 m_e$ and six with $m^*_{db} \geqslant 0.55 m_e$, giving a total density-of-states effective mass, including Fermi pocket degeneracy, of $m^*_d \approx 1.7 \pm 0.2 m_e$ (m_e is the free electron mass). The lattice term dominates the thermal conductivity, and the electronic contribution in samples with both electrons and holes present is in turn dominated by the ambipolar term. The low thermal conductivity and very large hole mass of $AgSbTe_2$ make it a most promising *p*-type thermoelectric material.

DOI: 10.1103/PhysRevB.77.245204 PACS number(s): 72.20.Pa, 71.20.Mq

I. INTRODUCTION

$AgSbTe_2$ is the paradigm for the class of I-V-VI_2 compound "semiconductors" where the group V element is P, As, Sb or Bi, the group VI element S, Se or Te, and the group I element can be Cu, Ag or Au,[1] or alternatively an alkali metal.[2] Like PbTe, $AgSbTe_2$ crystallizes in the rock-salt structure[3] with a similar lattice constant ($a=0.6462$ for PbTe and $a/2=0.6076$ nm for $AgSbTe_2$). It is also isoelectronic with PbTe in which the lead atom has a 2+ valence, and is replaced in $AgSbTe_2$ by one Ag^{1+} and one Sb^{3+}. The first pure ternary I-V-VI_2 compounds were identified[4] as chalcopyrites related to zinc-blende structures. By 1957, rock-salt $AgSbSe_2$ and $AgSbTe_2$ were synthesized,[5] and tentatively identified as narrow-gap semiconductors. Arrhenius plots of the temperature dependence of the resistivity have yielded energy gap values ranging from 0.6 to 0.2 eV. A structural study[6] of $AgSbTe_2$ identified a complicated microstructure in the early samples. An accompanying galvanomagnetic and thermoelectric study[7] showed that some samples can have positive and some negative Hall coefficients while maintaining a positive Seebeck coefficient: Clearly these early materials were inhomogeneous, and the properties of electrons and holes in intrinsic material were undetermined. To our knowledge, fundamental studies of the electronic properties of these semiconductors essentially came to a halt at that point because of these difficulties in the sample preparation, and surprisingly little is known about the simple ternary I-V-VI_2 compounds.

Rosi *et al.*[8] recognized the potential of $AgSbTe_2$ as a thermoelectric material: It is the bulk *p*-type thermoelectric with the highest figure of merit *ZT* (Ref. 9) of all simple ternary materials,[10] $ZT=1.3$ at 720 K, a temperature range relevant to applications in electrical power generation that use solar heat or fossil fuel combustion as a heat source. Unlike most materials used in thermoelectric power generation, $AgSbTe_2$ is lead-free and thus environmentally friendly. Alloys of $AgSbTe_2$ and $AgBiTe_2$ with PbTe,[8,11] SnTe (Refs. 8 and 11) and GeTe (Ref. 12) are well-studied thermoelectric materials.[8] The recently reported $AgPb_mSbTe_{2+m}$ bulk alloys[13] have $ZT=1.7$ at 750 K. At first sight,[8,11,12] they can be considered as solid solutions of $AgSbTe_2$ with PbTe, although this view is clearly oversimplified.[14]

Very recent band structure calculations[15] on $AgSbTe_2$ show the dependence of the energy band structure on the ordering of the metal (I-V) sublattice. Recent work finds evidence of Ag-Sb ordering;[14] and the calculations show that the lowest energy structure is one where the Ag and Sb atoms are ordered, the unit cell is fcc and double that of the PbTe structure. This structure is calculated to be a semimetal, with electrons in two sets of PbTe-like ellipsoidal pockets at the *L*-point of the Brillouin zone and the holes in two sets of six pill-box shaped half-pockets near the *X*-points. All calculated structures remain semimetallic[15] when the Ag-Sb disorder is increased. These calculations stand in contrast to the early experimental studies that identify the material as a semiconductor with a band gap of 0.2 to 0.6 eV. It must be noted that the calculations used the density functional theory which tends to underestimate energy gaps, and that these calculations do not establish conclusively that $AgSbTe_2$ is not a narrow-gap semiconductor. The present work addresses that question experimentally.

In this paper, we first present results on the longitudinal and transverse galvanomagnetic and thermomagnetic transport coefficients of polycrystalline $AgSbTe_2$ samples with a low carrier concentration and high electron mobility. The samples display two-carrier conduction. Using analysis techniques inspired by work on other semimetals, Bi (Refs. 16 and 17) and doped Bi (Ref. 18) in particular, we show here experimentally that $AgSbTe_2$ is, in fact, a semiconductor with a very narrow energy gap, on the order of meV at low temperature. We then use the quantum oscillations observed

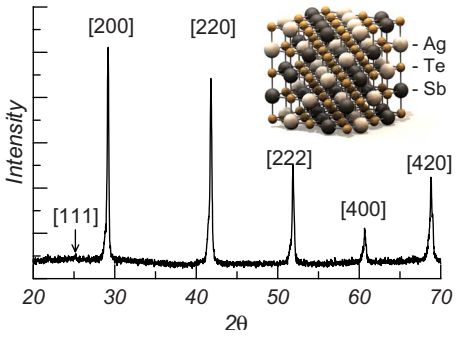

FIG. 1. (Color online) Powder x-ray diffraction spectrum of the ingot of $AgSbTe_2$ used in this work. The insert shows the AF-IIb structure (Ref. 15) with ordering of Ag and Sb in metallic sublattice.

in the magnetic susceptibility (the de Haas-van Alphen effect) of a single-crystal sample to determine the cross sections of the hole Fermi surface at 5 K; these are consistent with the band structure calculations for the ternary compound with Ag-Sb ordering of type AF-IIb[15] shown in Fig. 1. We do not have enough accuracy in either data or model to resolve the band parameters' temperature dependence, even though it is known that energy gaps in most narrow-gap semiconductors can change by values on the order of 100 meV between 4 K and 300 K.[19]

II. EXPERIMENT

Several ingots of $AgSbTe_2$ were prepared using conventional solid-state chemistry similar to the technique used for PbTe.[20] The ingots were polycrystalline, with crystallites exceeding a few mm on the side; the crystallites tend to grow preferentially along the $\langle 111 \rangle$ axis. An x-ray powder diffraction spectrum of the ingot used here most is shown in Fig. 1: The data show no presence of any second phase and a clean rock-salt structure with the correct lattice constant. The thermopower was uniform along the ingots, with several samples cut from the same ingot giving a repeatability of 2 to 3%; the ingot-to-ingot repeatability was 20%. We also have control over the carrier density in a limited range.

The de Haas-van Alphen oscillations in the magnetic susceptibility were measured in a superconducting quantum interference device magnetometer at 5 K on the single-crystal piece cut from the main ingot. One $2 \times 2 \times 1$ mm crystallite was cut from the ingot and oriented along its $\langle 111 \rangle$ axis. The magnetic field was oriented parallel to this axis and varied from 3 to 5.2 Tesla. The thermal, thermoelectric and thermomagnetic transport data were measured using the conventional static heater-and sink method, the galvanomagnetic data using DC current and a nanovoltmeter on a polycrystalline sample. The samples for transport measurements were cut as parallelepipeds from the ingots using a diamond saw, and deliberately kept small in order to minimize the effects of potential inhomogeneities. The typical dimensions of samples used for thermomagnetic and galvanomagnetic measurements were $1 \times 1 \times 8$ mm; two samples cut from one ingot, and one sample from a different ingot were measured. The data were very consistent and only one set is reported here, taken on a sample with dimensions of $(1.53 \pm 0.01) \times (0.90 \pm 0.01) \times \sim 8$ mm^3, with the distance between the longitudinal voltage probes 4.5 ± 0.2 mm. The electronic transport properties were taken from 77 to 400 K in magnetic fields from −2 to 2 Tesla. The cubic symmetry of the samples implies that polycrystalline samples are adequate for the analysis and that no Umkehr effects are expected; therefore the results can be deduced from data taken in both field polarities. The transverse effects (Hall and transverse Nernst–Ettingshausen coefficients) are extracted as the components that are odd with field, while longitudinal effects (magnetoresistance and magnetoseebeck effects) are extracted from the relevant even components. We report the isothermal thermomagnetic effects deduced from the measured adiabatic ones using the conventional methods.[21] Further in this text, we will label as "Nernst coefficient" the isothermal transverse Nernst–Ettingshausen coefficient. The thermal conductivity data were taken on several samples with a larger cross-section cut from neighboring regions of the ingot, in order to maintain thermal conductance around 4 mW/K. The sample on which the thermal conductivity data are reported here was $3.80 \times 3.75 \times 1.75$ mm^3, with the distance between the temperature probes 1.75 ± 0.03 mm. While radiative heat exchange was minimized by the use of radiation shields to below 0.4 mW/K, it was not corrected for.

The inaccuracy in sample dimensions, particularly in the distance between the longitudinal probes, is the main source of experimental inaccuracy. Consequently, the relative error on the electrical resistivity is on the order of 10%. The Hall coefficient depends only on the transverse dimension and is much more accurate (2%). The magnetoresistance is a relative value and does not depend directly on the geometry; however, there is a geometrical magnetoresistance[22] induced by the deflection of the current flux due to the Lorentz force near the contacts, on the order of a fraction (about 10% in the geometry used here) of μB (~0.4 for electrons at 300 K in these samples, see later), resulting in about a 4% total error. The two-carrier analysis presented further depends on both longitudinal and transverse magnetoconductances and thus carries through both errors on the longitudinal data, for a total of ~10%. This error reflects directly on the properties of the majority carrier. The inaccuracy is similar for the density of the minority carriers (electrons) which dominate the Hall coefficient, but it is larger for the electron mobility. The Seebeck coefficient does not depend on the sample geometry, and is thus more accurately measured. The main source of inaccuracy is the sample uniformity, limiting the accuracy of the Seebeck coefficient measurement to 3%. The magnetoseebeck effect is also subject to geometrical effects[23,24] again on the order of 4%. This renders the difference $S(B) - S(B = 0)$ inaccurate; it is reported for completion, but not used in the analysis. The Nernst data are afflicted by the 10% inaccuracy in the longitudinal distance between the temperature probes. The accuracy on the thermal conductivity is again limited by the geometry, but is somewhat better defined as the thermocouples were anchored to the top and bottom faces of the sample, the distance between which is easier to measure; the accuracy is estimated to be 5%.

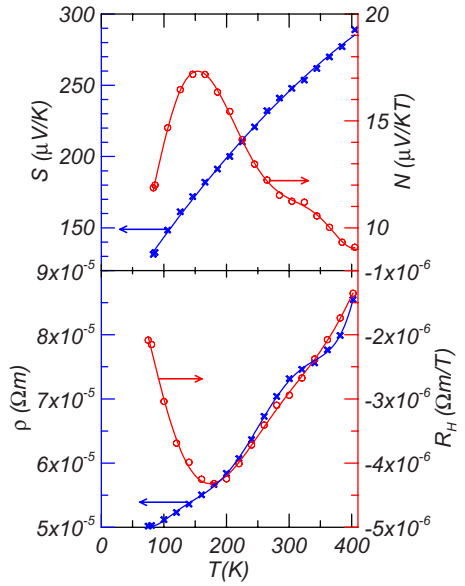

FIG. 2. (Color online) Experimental temperature dependence of the zero-field resistivity and Seebeck coefficients (×), and of the low-field Hall and Nernst (○) coefficients of one sample of $AgSbTe_2$. The lines are guides to the eye.

III. GALVANOMAGNETIC AND THERMOMAGNETIC TRANSPORT COEFFICIENTS

The galvanomagnetic and thermomagnetic data are shown as a function of temperature at zero magnetic field in Fig. 2, and as a function of magnetic field in Fig. 3 at a few selected temperatures. In Fig. 2, we show the zero-field resistivity and thermoelectric power or Seebeck coefficient. In Fig. 3 we show the magnetic field dependence of the magnetoresistive coefficient, defined as $\Delta\rho/\rho \equiv \rho(B)/\rho(B=0)-1$, and the magnetoseebeck coefficient defined as $\Delta S/S \equiv S(B)/S(B=0)-1$, where ρ and S are the longitudinal resistivity

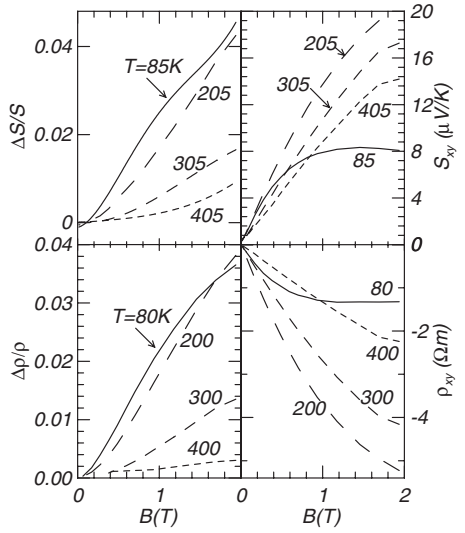

FIG. 3. Experimental magnetic field dependence of the relative magnetoresistance $\Delta\rho/\rho$, magnetoseebeck effect $\Delta S/S$, transverse Hall resistivity ρ_{xy}, and transverse Nernst thermopower S_{xy}. The data are only shown at the few selected temperatures indicated.

$\rho=\rho_{xx} \equiv E_x(B_z)/j_x$ and thermoelectric power $S=S_{xx} \equiv E_x(B_z)/\nabla T_x$, with the electric field parallel to the current or thermal flow direction x, in a transverse magnetic field z. Also shown in Fig. 3 are the transverse coefficient, the Hall resistivity ρ_{xy} and Nernst thermopower S_{xy}, taken with the electric field normal to both the current or heat flow, and to the magnetic field, i.e., by definition $\rho_{xy} \equiv E_y(B_z)/j_x$ and $S_{xy} \equiv E_y(B_z)/\nabla T_x$. The Hall coefficient in Fig. 2 is the zero-field slope of ρ_{xy}, and the transverse Nernst coefficient that of S_{xy}: $R_H \equiv \lim_{B_z\to 0}(\partial\rho_{xy}/\partial B_z)$ and $N \equiv \lim_{B_z\to 0}(\partial S_{xy}/\partial B_z)$.

The analysis of the data follows the classical method used on galvanomagnetic and thermomagnetic data of semimetals, such as doped bismuth,[18] arsenic,[25] and graphite.[26] The basic idea is to use the magnetic field dependence of the resistivity, magnetoresistance, and Hall effect to determine the partial electron and hole densities and mobilities. In a second step, the Seebeck and Nernst effects are used to deduce the Fermi energies in the electrons and hole Fermi surfaces. From the relation between these Fermi energies, it is possible to identify if the material is a semimetal or a semiconductor with a very small energy gap. The analysis is based on the following hypotheses:

(1) From the negative value of the Hall coefficient and the positive value of the Seebeck coefficient, one can deduce that the system has coexisting electrons and holes at all temperatures. The electrons most likely reside in one or more high-mobility low-mass bands that dominate the Hall coefficient; the holes reside in high-density-of-states mass bands whose partial Seebeck coefficient dominates the total thermopower. This image is also consistent with the calculated band structure.[15]

(2) Simple parabolic bands are assumed rather than Kane bands,[19] because the band structure calculations identify the potential very narrow energy gap to be indirect between the L- and X-points.

(3) The samples being large and of good quality, electrons are assumed scattered by acoustic phonons, resulting in an energy-dependence of the relaxation time $\tau=\tau_0 E^{\lambda}$ with a scattering exponent $\lambda=-1/2$.

(4) The following partial properties are defined for the electrons and holes, respectively: densities n and p (all positive), mobilities μ_e and μ_h (positive), electrical conductivities σ_e and σ_h (positive), partial Seebeck coefficients S_e (negative) and S_h (positive). The low-field transverse partial coefficients are partial Nernst coefficients[27] N_e and N_h, and partial Hall coefficient given by $R_{He}=-1/ne$ and $R_{Hh}=1/pe$. The latter formulation is an approximation which neglects the effect of the scattering exponent on the Hall coefficient and the anisotropy of the carriers' Fermi pockets, but its numerical effect on PbTe-type semiconductors is less than 10%, and will be accepted here by analogy.

(5) Unlike the case of the elemental group V semimetals (Bi, Sb and As) or graphite, $AgSbTe_2$ cannot be assumed to have an equal number of electrons and holes ($n \neq p$) as the ratio between the group I-B and group V element, or nonstoichiometries between the sum of these and the chalcogen, will result in excess electrons or holes. In practice, all the samples produced to date are dominantly p-type, which is most likely due to Ag vacancies.[15] The samples are expected to behave like doped semiconductors or semimetals.[18]

(6) The carriers will be assumed to have density-of-states effective masses m_d^* defined in such a way as to include the degeneracy of the Fermi pockets.

A. Analysis of the galvanomagnetic coefficients

In the presence of a transverse magnetic field along the z-axis, $B_z=B$, the longitudinal electrical resistivity $\rho_{xx}(B)$ and transverse (Hall) resistivity $\rho_{xy}(B)$ are the diagonal and off-diagonal elements of the equivalent conductivity elements $\sigma_{xx}(B_Z)$ and $\sigma_{xy}(B_Z)$ are given by

$$\rho_{xx}=\frac{\sigma_{xx}}{\sigma_{xx}^2+\sigma_{xy}^2},\quad \rho_{xy}=\frac{\sigma_{xy}}{\sigma_{xx}^2+\sigma_{xy}^2}, \tag{1}$$

where, in the presence of two types of carriers, electrons and holes, we have, with $B=B_z$:

$$\sigma_{xx}=\frac{ne\mu_e}{1+\mu_e^2B^2}+\frac{pe\mu_h}{1+\mu_h^2B^2},\quad \sigma_{xy}=\frac{-ne\mu_e^2B}{1+\mu_e^2B^2}+\frac{pe\mu_h^2B}{1+\mu_h^2B^2}. \tag{2}$$

A Taylor expansion of the magnetoresistance $\Delta\rho/\rho$ and of the Hall coefficient R_H around $B=0$, and valid for the intermediate-field regime where $\mu B\leq 2$, gives:

$$\frac{\Delta\rho}{\rho}(B)\equiv\frac{\rho_{xx}(B)}{\rho_{xx}(0)}-1=AB^2+CB^4,\quad A=\frac{(n\mu_e+p\mu_h)(n\mu_e^3+p\mu_h^3)-(-n\mu_e^2+p\mu_h^2)^2}{(n\mu_e+p\mu_h)^2},$$

$$C=\frac{-(n\mu_e+p\mu_h)(n\mu_e^5+p\mu_h^5)-(n\mu_e^3+p\mu_h^3)^2+2(-n\mu_e^2+p\mu_h^2)}{(n\mu_e+p\mu_h)^2}$$

$$-\frac{n\mu_e p\mu_h(\mu_e^2+\mu_h^2+2\mu_e\mu_h)[(-n\mu_e^2+p\mu_h^2)-2(n\mu_e+p\mu_h)(n\mu_e^3+p\mu_h^3)]}{(n\mu_e+p\mu_h)^4}, \tag{3}$$

and:

$$\rho_{xy}(B)=R_HB+DB^3,\quad R_H\equiv\lim_{B_z\to 0}(\partial\rho_{xy}/\partial B_z)=\frac{-n\mu_e^2+p\mu_h^2}{(n\mu_e+p\mu_h)^2},$$

$$D=-\frac{(-n\mu_e^4+p\mu_h^4)}{(n\mu_e+p\mu_h)^2}-\frac{(-n\mu_e^2+p\mu_h^2)[(-n\mu_e^2+p\mu_h^2)^2-2(n\mu_e+p\mu_h)(n\mu_e^3+p\mu_h^3)]}{(n\mu_e+p\mu_h)^4}. \tag{4}$$

Fitting at each temperature $\rho=\rho_{xx}(B=0)$ and R_H from Fig. 3, as well as A, C, and D deduced from Fig. 3, makes it possible to deduce n, p, μ_e, and μ_h and thus the partial electron and hole conductivities at $B=0$:

$$\sigma_e=ne\mu_e,\quad \sigma_h=pe\mu_h,\quad \sigma=1/\rho=\sigma_e+\sigma_h. \tag{5}$$

The results are shown Fig. 4. At room temperature, the sample has about $n\approx 10^{17}$ cm^{-3} high-mobility ($\mu_e\approx 2200$ cm^2/Vs) electrons that are most likely thermally activated. It also contains $p\approx 5\times 10^{19}$ cm^{-3} low-mobility ($\mu_e\approx 11$ cm^2/Vs) holes. The hole density at 77 K is $\approx 4\times 10^{19}$ cm^{-3} and extrapolates to 3×10^{19} cm^{-3} at 0 K, where the electrons freeze out. This charge unbalance must be due to a departure from stoichiometry, possibly related Ag vacancies as discussed above. While in nondegenerate semiconductors it would be possible to deduce an energy gap from the temperature dependence of the "intrinsic" carrier density n_i defined by $n_i\equiv\sqrt{np}$, applying that analysis to the present data would give $E_g=0$ meV, which invalidates the assumption that the semiconductor is nondegenerate: The thermoelectric and thermomagnetic data contain experimental information that will enable the determination of the Fermi level and the energy gap.

B. Analysis of the thermomagnetic coefficients

In two-carrier systems, the Seebeck coefficient is given as a function of the partial electron and hole Seebeck coefficients by:[28]

$$S=\frac{S_e\sigma_e+S_h\sigma_h}{\sigma_e+\sigma_h} \tag{6}$$

and the low-field Nernst coefficient by:

$$N=\frac{(N_e\sigma_e+N_h\sigma_h)(\sigma_e+\sigma_h)+(S_h-S_e)(R_{Hh}\sigma_h-R_{He}\sigma_e)\sigma_e\sigma_h}{(\sigma_e+\sigma_h)^2}. \tag{7}$$

Expressions for the partial Seebeck and Nernst coefficients are given as functions of the Fermi energy in the conduction and valence bands, E_{Fe} and E_{Fh}. They have the form of the well-known transport integrals, which for parabolic bands are given as a function of the Fermi integral $F_j(\xi)$:[29]

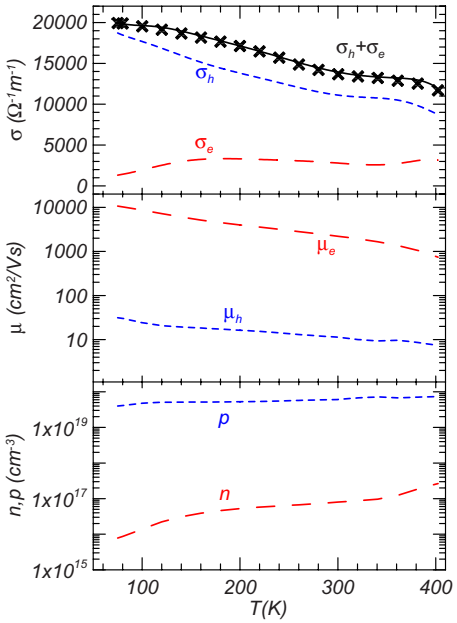

FIG. 4. (Color online) Fitted electron (dashed lines) and hole (dotted lines) densities (n,p), mobilities (μ_e,μ_h) and partial electrical conductivities (σ_e,σ_h) as a function of temperature. Also shown are the total calculated conductivity compared to experimental values $(\times)$.

$$F_j(\xi) \equiv \int_0^\infty \frac{x^j dx}{1+\exp(x-\xi)},$$

$$S_e = -\frac{k_B}{e}\left[\frac{\left(\frac{5}{2}+\lambda\right)F_{3/2+\lambda}(\xi_e)}{\left(\frac{3}{2}+\lambda\right)F_{1/2+\lambda}(\xi_e)} - \xi_e\right],$$

$$S_h = \frac{k_B}{e}\left[\frac{\left(\frac{5}{2}+\lambda\right)F_{3/2+\lambda}(\xi_h)}{\left(\frac{3}{2}+\lambda\right)F_{1/2+\lambda}(\xi_h)} - \xi_h\right],$$

$$N_e = \frac{k_B}{e}\left[\frac{\left(\frac{5}{2}+2\lambda\right)F_{3/2+\lambda}(\xi_e)}{\left(\frac{3}{2}+2\lambda\right)F_{1/2+\lambda}(\xi_e)} - \frac{\left(\frac{5}{2}+\lambda\right)F_{3/2+\lambda}(\xi_e)}{\left(\frac{3}{2}+\lambda\right)F_{1/2+\lambda}(\xi_e)}\right],$$

$$N_h = \frac{k_B}{e}\left[\frac{\left(\frac{5}{2}+2\lambda\right)F_{3/2+\lambda}(\xi_h)}{\left(\frac{3}{2}+2\lambda\right)F_{1/2+\lambda}(\xi_h)} - \frac{\left(\frac{5}{2}+\lambda\right)F_{3/2+\lambda}(\xi_h)}{\left(\frac{3}{2}+\lambda\right)F_{1/2+\lambda}(\xi_h)}\right]. \quad (8)$$

In these expressions, λ is the scattering exponent representing the energy-dependence of the relaxation time, defined by $\tau=\tau_0 E^\lambda$. In the following analysis, we assume that acoustic phonon scattering $(\lambda=-1/2)$ dominates at all temperatures, in order to minimize the number of adjustable parameters. The reduced Fermi energies are given by $\xi \equiv E_F/k_BT$, E_{Fe} and ξ_e for electrons as measured from the bottom of the conduction band and E_{Fh} and ξ_h for holes, as measured from the top of the valence band. If the material is a semimetal, the conduction and the valence band overlap each other by a small overlap energy E_o; the electron and hole Fermi energies are related by:

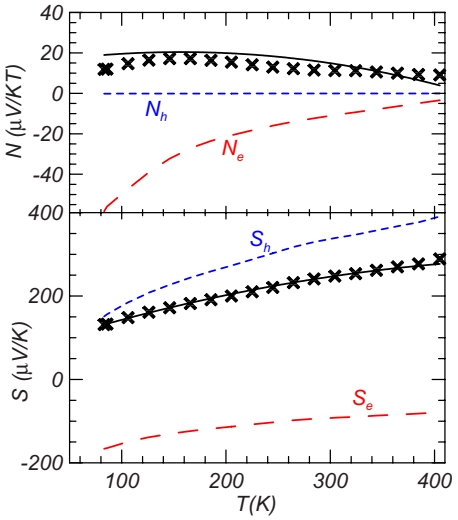

FIG. 5. (Color online) Fit of the zero-field Seebeck and of the low-field isothermal Nernst coefficients: the partial electron (dashed lines) and hole (dotted lines) thermopowers and Nernst coefficients are shown, alongside the calculated total (full lines), which can be compared to the data points $(\times)$. The fit assumes that only acoustic phonon scattering is present at all temperatures, and that the energy gap is temperature-independent; therefore the Nernst coefficient, which is very sensitive to the scattering mechanism, is reproduced with only moderate accuracy.

$$E_{Fe} = -(E_{Fh}+E_o), \quad \xi_e = -\xi_h - \frac{E_o}{k_BT}. \quad (9)$$

If, on the other hand, the material is a semiconductor with an energy gap E_g, we have:

$$E_{Fe} = -E_{Fh}+E_g, \quad \xi_e = -\xi_h + \frac{E_g}{k_BT}, \quad (10)$$

i.e., $E_g=-E_o$ and we can use the relations (9) and (10) to determine the nature of the material from the sign of E_o.

The next step is to fit the experimental Seebeck and Nernst coefficients using the partial conductivities from Fig. 4 and relations (6)–(9). In order to further limit the number of adjustable parameters, we assume that E_g has no temperature dependence, even though we know this to be a very rough approximation: The energy overlap in Bi varies by 100 meV between 77 and 300 K.[19] This leaves one adjustable parameter at each temperature, $E_{Fe}(T)$, and one parameter to be adjusted for all temperatures, E_o or E_g. Numerically, less importance is to be given to the Nernst coefficient than to the Seebeck coefficient, because the Nernst coefficient is known with only a 10% accuracy, and also is the transport coefficient that is most sensitive to the scattering exponent λ. The results of the fit are shown in Fig. 5, where we give the resulting values of S_e, S_h, N_e, N_h and the calculated values of S and N. S fits the data very well, as it was used to determine the Fermi energies E_{Fe} and E_{Fh} at each temperature. The optimal fit through N corresponds to an energy gap of $E_g = 7.6 \pm 3$ meV. We conclude that $AgSbTe_2$ is a semiconductor with a very narrow, almost zero, energy gap. The band structure calculations[15] show E_g is indirect with electrons at

the L-points and holes near the X-points of the Brillouin zone. The Fermi energy extrapolates to $E_{Fh}(T=0\ \mathrm{K})=15$ meV into the valence band at zero temperature.

The hole density is a function of the density-of-states effective mass m_d^* and the Fermi energy E_{Fh}; in degenerate statistics:

$$p = \frac{(2m_d^* E_{Fh})^{3/2}}{3\pi^2\hbar^3}. \tag{11}$$

It is possible to deduce the total density-of-states effective mass m_d^* from $E_{Fh}(T=0\ \mathrm{K})$ and the hole density extrapolated to 0 K of 3×10^{19} cm^{-3}, to obtain $m_d^*=2.2\pm0.6m_e$, where m_e is the free electron mass. This value includes the degeneracy of the hole Fermi surface pockets. We show in paragraph 4 that the hole mass value deduced here is confirmed by the de Haas-van Alphen oscillations. The same procedure applied at 77 K to the minority electrons using Fermi integrals gives a density-of-states mass of $\sim0.02m_e$, but this is not accurate because the electron partial Seebeck coefficient contributes only ~20% to the total Seebeck coefficient. Nevertheless, the product of the electron and hole density-of-states masses would give $\sim0.05m_e^2$, which is consistent with the calculated intrinsic carrier density n_i at 77 K, and the ratio of the hole mass to the electron mass is close to the inverse of that between the mobilities, a factor of 100–300. The electron density-of-states mass must be about two orders of magnitude smaller than the hole density-of-states mass.

C. Electronic and ambipolar thermal conductivity

The simultaneous presence of electrons and holes strongly suggests the presence of an ambipolar electronic thermal conductivity (κ_{AMBI}). In semimetals, a substantial amount of heat can be carried by this term: For example, up to 60% of the electronic thermal conductivity in the semimetal Bi is of this origin.[17] The ambipolar term arises because the heat flux carried by each carrier pocket is the sum of a thermal conductivity term and a Peltier term. In the presence of a temperature gradient, each carrier pocket gives rise to a partial Seebeck coefficient. When two or more carrier pockets are present, they can be considered connected in parallel, and the two unequal partial Seebeck voltages give rise to an electrical current flux "circulating" between the two-carrier pockets, which in turn creates partial Peltier heat fluxes in each. The balance of these partial Peltier heat fluxes adds to the thermal conductivity: Even though the electrical fluxes balance each other exactly to zero, the thermal fluxes always add, and flow along the temperature gradient, because the Peltier and Seebeck coefficients have the same sign. The ambipolar thermal conductivity is given by:[17]

$$\kappa_{\mathrm{AMBI}} = T\frac{\sigma_e\sigma_h}{\sigma_e+\sigma_h}(S_h-S_e)^2 \tag{12}$$

and is readily calculated from the data in Fig. 5. The value at room temperature, $\kappa_{\mathrm{AMBI}}=0.128$ W/mK, is a significant fraction of the experimental thermal conductivity in the sample studied.

The partial electron and hole thermal conductivities can be obtained by applying the Wiedemann–Franz law to the electron and hole partial electrical conductivities. The Lorenz ratios can be estimated from the Fermi integrals assuming acoustic phonon scattering; since the reduced Fermi energies are $-2<\xi_h<0.7$ and $0.4<\xi_e<2.6$, the calculated Lorenz ratios are on the order of 0.8 to 0.9 of the free electron value $L_0=\pi^2/3(k_B/e)^2$. This value is of the same order as that of the PbTe, where the experimental value is 0.6 to 0.8 L_0.[29] For that reason, and because the electronic thermal conductivities represent only a small contribution to the total, a value of $L\approx0.7L_0$ will be used further, giving electron and hole partial thermal conductivities of $\kappa_{el}=0.015$ W/mK and $\kappa_h=0.058$ W/mK at 300 K. The calculated temperature-dependent values of the different electronic terms are shown in Fig. 6. As was the case in Bi, the ambipolar thermal conductivity represents over 60% of the total electronic thermal conductivity at room temperature. The difference between the total thermal conductivity and the electronic contributions is attributed to the lattice, and is on the order of 0.65 W/mK at 300 K, in good agreement with the literature.[30] The lattice properties of this class of semiconductors will be discussed in a separate article.[31]

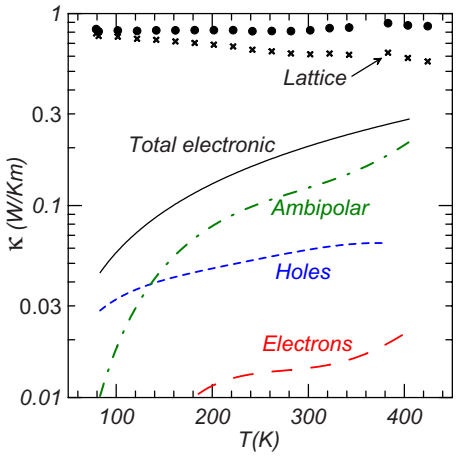

FIG. 6. (Color online) Experimental temperature dependence of the thermal conductivity of an $AgSbTe_2$ from the same ingot as was used for Figs. 2 and 3 (●). The ambipolar thermal conductivity (dashed-dotted line) dominates the total electronic contribution (full line), which contains estimates of the electron (dashed line) and hole (dotted line) contributions. The crosses are the difference between the experimental data points and the electronic contributions, and represent the lattice thermal conductivity.

IV. ANALYSIS OF THE DE HAAS-VAN ALPHEN OSCILLATIONS

Figure 7 (bottom frame) shows the magnetic field dependence of the oscillations in magnetic susceptibility of the single-crystal sample in a magnetic field aligned with its ⟨111⟩ axis, after the diamagnetic background is subtracted. The data are periodic when plotted versus inverse magnetic field $(1/B)$; a Fourier transform of such plot gives the amplitude of the Fourier components as a function of a "frequency" $1/\Delta[1/B]$, the inverse of a period $\Delta[1/B]$. The Fourier transform, shown in the upper frame of Fig. 7, identifies two frequencies, labeled a and b, at $1/\Delta[1/B]_a=25.9$ and at

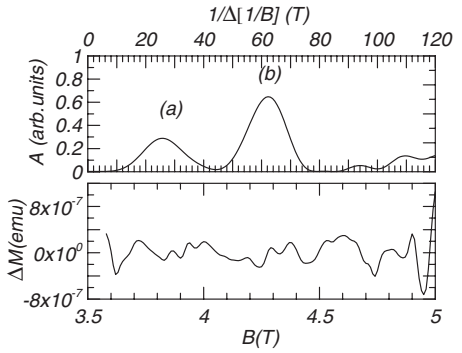

FIG. 7. De Haas-van Alphen oscillations in the magnetic field dependence of the magnetic susceptibility, with the diamagnetic background subtracted, of a 4 mm^3 crystal of $AgSbTe_2$ oriented with the magnetic field along the $\langle 111\rangle$ axis at 5 K (bottom frame). The top frame shows the Fourier component amplitude of the oscillations plotted as a function of the inverse magnetic field frequency, identifying two frequencies at 25.9 and 62.0 Tesla.

$1/\Delta[1/B]_b = 62.0(T)$. These correspond to oscillations of holes in quantized orbits on the Fermi surfaces and give Fermi surface cross-sections A_F normal to the $\langle 111\rangle$ direction via:

$$A_F = \frac{2\pi e}{\hbar}\frac{1}{\Delta[1/B]}, \tag{13}$$

to yield $A_{Fa} = 2.47 \times 10^{17}$ m^{-2} and $A_{Fb} = 5.93 \times 10^{17}$ m^{-2}.

These experimental values can be compared to the Fermi-surface cross sections estimated from the band structure calculations, using the Fermi level position deduced from the thermomagnetic data in paragraph 3, to $E_{Fh}(T=0\ \mathrm{K}) = 15$ meV. The hole Fermi surfaces corresponding to the band structure calculations of K. Hoang *et al.*[15] are shown in Fig. 8 (after K. Hoang[32]); the two pockets in Figs. 8(a) and 8(b) centered near the X-point of the Brillouin zone are filled in the sample studied here, while the third pocket centered on the Δ' point partially along the X-Γ axis is some 70 meV below the Fermi energy. Effective masses calculated[32] from the bending of the dispersion relations[15] along the X-W and X-Γ directions are given in Table I; given the rounded pill-box shape of the Fermi surfaces, an estimate for the density-of-states effective mass m^*_{da} and m^*_{db} of pockets (a) and (b) can be made and is also given in Table I. Finally, the Fermi-surface cross sections normal to the $\langle 111\rangle$ axis of each set of three (a) and (b) pockets are degenerate, and can be approximated by an ellipse with a cyclotron mass m^*_C given in Table I. Using the Fermi energy $[E_{Fh}(T=0\ \mathrm{K}) = 15\ \mathrm{meV}]$ deduced from the Seebeck coefficient, it is finally possible to calculate the cross-sections A_{Fa} and A_{Fb} of the two pockets in the sample measured, also shown in Table I. These cross sections compare very well to the ones deduced from the de Haas-van Alphen measurements, thus confirming the entire picture for the valence band. One more verification can be made: From the calculated values of the density-of-states mass m^*_{da} and

TABLE I. Calculated hole effective masses (in units of the free electron mass m_e) of the two pockets (a) and (b) shown in Fig. 8 along two directions. From these, the density-of-states mass m^*_{da} and m^*_{db} of the different pockets are deduced, and the cyclotron mass m^*_C that corresponds to an elliptical orbit normal to the $\langle 111\rangle$ direction of cross section equivalent to that of the actual pocket. The hole Fermi surface cross-sections A_F (in units of 10^{17} m^{-2}) of pockets (a) and (b) are calculated from m^*_C using a Fermi energy of 15 meV, and is compared to the experimental cross-section deduced from the de Haas-van Alphen oscillations.

Mass	Pocket *a*	Pocket *b*
$m^*_{X\Gamma}$ [a]	0.109 ± 0.003	0.144 ± 0.004
m^*_{XW} [a]	0.332 ± 0.004	1.36 ± 0.02
m^*_d per pocket	0.21 ± 0.01	0.57 ± 0.02
$m^*_C\langle 111\rangle$	0.25	0.52
A_F (E_F=15 meV)	3.02	6.2
A_F experimental	2.47	5.93

[a]Reference 32.

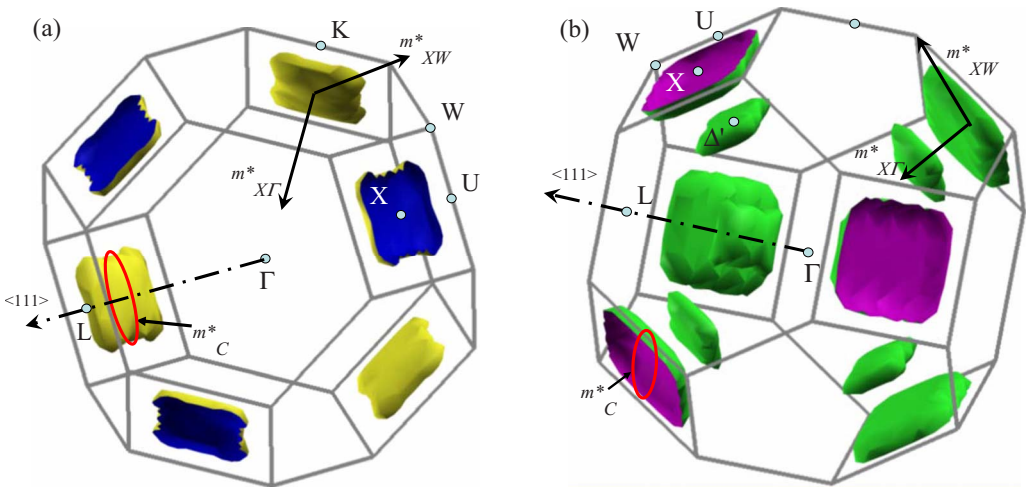

FIG. 8. (Color online) Calculated hole Fermi surfaces for $AgSbTe_2$ per Ref. 32 with Ag and Sb atoms ordered on the metal sublattice, case AF-IIb. The small pockets around Δ' are not populated in the sample studied here; the masses for the other pockets are given in Table I along the directions indicated.

m_{db}^* of each pocket, and given a degeneracy factor of 3 for each pocket type, we can calculate a total density-of-states mass for the valence band as $m_d^*=3^{2/3}(m_{da}^{*3/2}+m_{db}^{*3/2})^{2/3} \approx 1.5\pm 0.2m_e$, quite consistent with the value of $2.2\pm 0.6m_e$ deduced from the Seebeck and Hall coefficients. Since the accuracy of the de Haas-van Alphen measurements is superior to that of the transport measurements, and the cyclotron masses correspond quite well to the calculated masses, we attach more weight to the quantum oscillation experiments and determine a density-of-states hole mass of $m_d^* =1.7\pm 0.2m_e$.

V. CONCLUSIONS

In conclusion, $AgSbTe_2$ is a semiconductor with a very narrow energy gap (~ 7 meV), highly mobile electrons that dominate the Hall measurements, and holes in a heavy band that dominate the thermoelectric power. Since the gap energy becomes comparable to the thermal energy k_BT for temperatures above 100 K, $AgSbTe_2$ can in practice be considered as an indirect zero-gap material above that temperature. Preliminary values for the density-of-states effective mass for holes is $m_d^*=1.7\pm 0.2m_e$, consistent with the calculated bands of the AF-IIb structure, with FCC symmetry, of Hoang *et al.*,[15] and suggest that Ag and Sb atoms order in the metal sublattice. In the AF-IIb band structure, the hole Fermi surface is expected to consist of two sets of threefold degenerate rounded pillboxes near the *X*-point of the Brillouin zone. The high density of excess holes (~ 3 to 4×10^{19} cm^{-3}) is presumably due to vacancies on the metal sites (Ag?) in our samples; the low and very temperature-dependent electron density is thermally excited across the gap. The thermal conductivity is dominated by the lattice but can have an important ambipolar contribution. The low lattice thermal conductivity and the large density-of-states hole mass make the material a promising *p*-type thermoelectric semiconductor.

ACKNOWLEDGMENTS

This work was supported by a grant from BSST, by NSF Grant No. CBET-0754023, and partially by the Ohio Department of Development Wright Center for Photovoltaic Innovation and Commercialization. We would like to acknowledge S. D. Mahanti and K. Hoang and thank them for sharing unpublished data.

[1] V. P. Zhuze, V. M. Sergeeva, and E. L. Shtrum, Sov. Phys. Tech. Phys. **3**, 1925 (1958).
[2] V. A. Bazakutsa and M. P. Vasilieva, J. Eng. Phys. **34**, 137 (1978).
[3] S. Geller and J. H. Wernick, Acta Crystallogr. **12**, 46 (1959).
[4] C. H. L. Goodman and R. W. Douglas, Physica (Amsterdam) **20**, 1107 (1954).
[5] J. H. Wernick and K. E. Benson, Phys. Chem. Solids **3**, 157 (1957).
[6] R. W. Armstrong, J. W. Faust, Jr., and W. A. Tiller, J. Appl. Phys. **31**, 1954 (1960).
[7] R. Wolfe, J. H. Wernick, and S. E. Haszko, J. Appl. Phys. **31**, 1959 (1960).
[8] F. D. Rosi, E. F. Hockings and N. E. Lindenblad, RCA Rev. **22** 121 (1961).
[9] The thermoelectric figure of merit is a measure of the efficiency of thermoelectric devices, and is defined as $Z=S^2\sigma/\kappa$, where S is the thermoelectric power or Seebeck coefficient, σ is the electrical conductivity, and κ is the thermal conductivity. It is customary to express the figure of merit as the unitless product of Z with the average operating temperature T. As most thermoelectric materials are semiconductors in which κ is dominated by lattice conduction, it is also customary to group the electronic contributions into the "power factor" $P=S^2\sigma$.
[10] C. Wood, Rep. Prog. Phys. **51**, 459 (1988).
[11] H. Fleischmann, O. G. Folberth, and H. Pfister, Z. Naturforsch. A **14A**, 999 (1959).
[12] H. Fleischmann, H. Luy, and J. Rupprecht, Z. Naturforsch. A **18A**, 646 (1963).
[13] K. F. Hsu, S. Loo, F. Guo, W. Chen, J. S. Dyck, C. Uher, T. Hogan, E. K. Polychroniadis, and M. G. Kanatzidis, Science **303**, 818 (2004).
[14] E. Quarez, K.-F. Hsu, R. Pcionek, N. Frangis, E. K. Polychroniadis, and M. G. Kanatzidis, J. Am. Chem. Soc. **127**, 9177 (2005).
[15] K. Hoang, S. D. Mahanti, J. R. Salvador, and M. G. Kanatzidis, Phys. Rev. Lett. **99**, 156403 (2007).
[16] B. Abeles and S. Meiboom, Phys. Rev. **101**, 544 (1956).
[17] C. F. Gallo, B. S. Chandrasekhar, and P. H. Sutter, J. Appl. Phys. **34**, 144 (1963).
[18] J. Boxus, J. Heremans, J.-P. Michenaud, and J.-P. Issi, J. Phys. F: Met. Phys. **9**, 2387 (1979).
[19] J. Heremans and O. P. Hansen, J. Phys. C **16**, 4623 (1983).
[20] J. P. Heremans, C. M. Thrush, and D. T. Morelli, J. Appl. Phys. **98**, 063703 (2005).
[21] J. P. Heremans, C. M. Thrush, and D. T. Morelli, Phys. Rev. B **70**, 115334 (2004).
[22] Daniel R. Baker and Joseph P. Heremans, Phys. Rev. B **59**, 13927 (1999).
[23] J. P. Heremans, C. M. Thrush, and D. T. Morelli, Phys. Rev. Lett. **86**, 2098 (2001).
[24] J. P. Heremans, C. M. Thrush and D. T. Morelli, Phys. Rev. B **65**, 035209 (2001).
[25] J. Heremans, J.-P. Issi, A. A. M. Rashid, and G. A. Saunders, J. Phys. C **10**, 4511 (1977).
[26] J. Heremans, J.-P. Issi, I. Zabala-Martinez, M. Shayegan, and M. S. Dresselhaus, Phys. Lett. **84A**, 387 (1981).
[27] Equation (7) shows that the total Nernst coefficient in a two-carrier system is in fact a very strong function of the partial Seebeck coefficients rather than the partial Nernst coefficients alone.
[28] E. H. Putley, *The Hall Effect and Semiconductor Physics* (Dover, New York, 1968).
[29] Yu. I. Ravich, B. A. Efimova, and I. A. Smirnov, *Semiconducting Lead Chalcogenides* (Plenum, New York, 1970).
[30] E. F. Hockings, Phys. Chem. Solids **10**, 341 (1959).
[31] D. T. Morelli, V. Jovovic, and J. P. Heremans, Phys. Rev. Lett. (to be published).
[32] K. Hoang, Ph.D. thesis, Michigan State University, 2007.